Environment International 156 (2021) 106638

Contents lists available at ScienceDirect

Environment International

journal homepage: www.elsevier.com/locate/envint

Mechanistic insights into the (im)mobilization of arsenic, cadmium, lead, and zinc in a multi-contaminated soil treated with different biochars

Ali El-Naggar [a,b,c], Scott X. Chang [c,d], Yanjiang Cai [c], Young Han Lee [e], Jianxu Wang [f,g], Shan-Li Wang [h], Changkook Ryu [i], Jörg Rinklebe [g,j,**], Yong Sik Ok [a,*]

[a] Korea Biochar Research Center, APRU Sustainable Waste Management Program & Division of Environmental Science and Ecological Engineering, Korea University, Seoul 02841, Republic of Korea
[b] Department of Soil Sciences, Faculty of Agriculture, Ain Shams University, Cairo 11241, Egypt
[c] State Key Laboratory of Subtropical Silviculture, Zhejiang A & F University, Lin'an 311300, China
[d] Department of Renewable Resources, University of Alberta, Edmonton, Alberta T6G 2H1, Canada
[e] Division of Environmental Agriculture Research, Gyeongsangnam-do Agricultural Research & Extension Services, Jinju 52773, Republic of Korea
[f] State Key Laboratory of Environmental Geochemistry, Institute of Geochemistry, Chinese Academy of Sciences, Guiyang 550081, China
[g] University of Wuppertal, School of Architecture and Civil Engineering, Institute of Foundation Engineering, Water- and Waste-Management, Laboratory of Soil- and Groundwater-Management, Pauluskirchstraße 7, 42285 Wuppertal, Germany
[h] Department of Agricultural Chemistry, National Taiwan University, Taipei 10617, Taiwan, ROC
[i] School of Mechanical Engineering, Sungkyunkwan University, Suwon 16419, Republic of Korea
[j] Department of Environment, Energy, and Geoinformatics, Sejong University, Seoul 05006, Republic of Korea

ARTICLE INFO

Handling Editor: Yong-Guan Zhu

Keywords:
Biochar feedstock
Charcoal
Sustainable remediation
Soil contamination
Soil remediation
XANES
XPS
Food safety

ABSTRACT

The effect and mechanistic evidence of biochar on the (im)mobilization of potentially toxic elements (PTEs) in multi-contaminated soils, with respect to the role of surface-functional groups and organic/inorganic compounds of biochar, are poorly understood. Herein, biochars produced from grass residues, rice straw, and wood were applied to a mining-soil contaminated with As, Cd, Pb, and Zn for 473-d. Biochars did not reduce the mobilization of Cd and Zn, whereas they simultaneously exhibited disparate effects on As and Pb mobilization. The phenolic hydroxyl and carboxylic groups on the wood biochar's surfaces promoted the conversion of Pb^{2+} into $PbCO_3$/$Pb(OH)_2$ and/or PbO, minimally by the rice and grass biochars. Rice and grass biochars led to the dissolution of scorodite and the formation of less stable forms of Fe-oxide-bound As (i.e., goethite and ferrihydrite); furthermore, it resulted in the reduction of As(V) to As(III). The PTEs mobilization and phytoavailability was mainly governed by the release of dissolved aliphatic- and aromatic-carbon, chloride, sulfur chemistry, phosphate competition, and the electrostatic repulsion in biochar-treated soils. In conclusion, pristine-biochar has a limited impact on the remediation of multi-contaminated soils, and the use of modified-biochar, possessing higher surface areas and functionality and active exchange sites, are preferred under such conditions.

1. Introduction

The United Nations called for urgent action on remediation of the contaminated ecosystems, in order to achieve the Sustainable Development Goals (SDGs) (Hou et al., 2020). Mining and smelting activities drive the prolonged environmental contamination of surrounding soils due to the translocation of potentially toxic elements (PTEs) via airborne mining dust, tailings, and surface runoff from mining drainage (Masto et al., 2019). Consequently, contaminated soils adjacent to mining sites pose a major health concern when they are utilized in agricultural activities and food production for human consumption (Masto et al., 2019; Monteiro et al., 2019). The high environmental risk further elevates with the transfer of PTEs like As, Cd, Pb, and Zn, to groundwater, plants, and the food chain (Rinklebe et al., 2019). Therefore, the *in situ* remediation of such soils using cost-effective and eco-friendly amendments to immobilize the PTEs in the soil has gained increasing interest within the framework of the SDGs implementation (Monteiro et al., 2019; Palansooriya et al., 2020).

* Corresponding author.
** Corresponding author.
E-mail addresses: rinklebe@uni-wuppertal.de (J. Rinklebe), yongsikok@korea.ac.kr (Y. Sik Ok).

https://doi.org/10.1016/j.envint.2021.106638
Received 12 November 2020; Received in revised form 7 April 2021; Accepted 9 May 2021
Available online 21 May 2021

Biochar has garnered significant attention for soil amendment, owing to its role in environmental remediation, as confirmed by the promising results of numerous studies (Ahmad et al., 2014; El-Naggar et al., 2019a; Igalavithana et al., 2019; Shaheen et al., 2019; You et al., 2017). The possible mechanisms for the immobilization of PTEs in biochar-treated soils include: (1) electrostatic attraction of cationic/anionic PTEs on biochar active sites, (2) physical adsorption on the internal surfaces of biochar pores, (3) surface (co)precipitation with the elements contained in biochar, and (4) complexation with biochar surface-functional groups, such as —COOH and —OH (Ahmad et al., 2014; El-Naggar et al., 2018a; Rajapaksha et al., 2016; Sun et al., 2019; Yuan et al., 2017). Therefore, the high porosity, large inner surface area, and diverse surface-functional groups afford biochar the potential to improve the remediation of contaminated soils near mining sites through the immobilization of PTEs.

However, the application of biochar to multi-contaminated soils has exhibited contrasting effects on remediating contamination. For instance, the application of poultry litter and soybean stover biochar to multi-contaminated soils decreased the mobility of Pb and Zn, but soybean stover biochar increased that of As (Ahmad et al., 2017; Lu et al., 2018); meanwhile, the application of peanut shell, eucalyptus wood, and pine needle biochars did not affect the mobility of As, Pb, and Zn (Ahmad et al., 2017; Lu et al., 2018). Many other recent studies reported that biochar application increased the potential mobility and/or phytoavailability of As, Cd, Pb, and Zn in multi-contaminated soils (Awad et al., 2018; Beiyuan et al., 2017; El-Naggar et al., 2019b; Shaheen et al., 2018); therefore, the ability of biochar for PTE immobilization in multi-contaminated soils remains to be fully elucidated.

It is anticipated that elevated concentrations of various PTEs in soil will drive a competition of toxic elements for the binding sites of biochar surfaces; this will prove challenging for biochar because of its limited adsorption capacity. Moreover, biochar-induced changes in the soil pH and the dissolved aliphatic and aromatic carbon, Fe, Mn, P, and S interactions are potential factors that might influence the geochemical process. Consequently, this has an impact on the (im)mobilization of PTEs in multi-contaminated soils. The evaluation of the efficacy of the biochar produced from different feedstocks for remediating degraded soils requires a better understanding of the controlling factors and mechanisms involved in biochar-multi PTE interactions. Although some studies have investigated the effects of biochar application on multi-contaminated soils (Ahmad et al., 2017; Lu et al., 2018; Pukalchik et al., 2018, 2017), few have studied the factors controlling the behavior of PTEs (Awad et al., 2018; Beiyuan et al., 2017; El-Naggar et al., 2019b). Moreover, the role of surface-functional groups of biochar derived from different feedstocks on the (im)mobilization of PTEs in multi-contaminated soils has not been systematically studied.

We hypothesized that: (1) the negatively charged acidic functional groups (e.g., phenol hydroxyl and carboxyl) on biochar surfaces can facilitate the dissolution of coprecipitated PTEs and exhibit competitive sorption for the multi-contaminants in soil, leading to lower PTE-retaining potential by the biochar in the soil; (2) biochar can increase the soil capacity for accepting/donating electrons, thus influencing the chemistry of Mn and Fe oxides, promoting their transformation to less stable forms. This will lead to an increase in the release potential of associated PTEs; (3) the potential mobility and phytoavailability of PTEs are mainly governed by the release of dissolved organic (aliphatic and aromatic) compounds, the strong association with S and P chemical structure, and the changes induced by biochar in them. Meanwhile, the hypothesis that the production of glomalin in biochar-treated soils might constrain the potential mobility and phytoavailability of PTE needs to be tested. In this study, we systematically elucidated the impact of biochars produced from grass residues, rice straw, and wood on the geochemical processes related to the potential mobility and phytoavailability of As, Cd, Pb, and Zn after 473 d of biochar addition to a multi-contaminated soil. The overall aim was to elucidate the controlling factors and mechanisms involved in the (im)mobilization of As, Cd, Pb, and Zn in a multi-contaminated soil treated with biochar produced from different feedstocks.

2. Materials and methods

2.1. Characterization of soil and biochar samples

A composite surface (0–20 cm) soil sample was collected from a mining site in Chungcheongnam-do, South Korea. The soil sample was air-dried, sieved (<2 mm), and characterized, as reported in El-Naggar et al. (2020). In brief, the soil exhibited a sandy loam texture (sand = 60%, silt = 31%, and clay = 9%), pH = 7.1, electrical conductivity (EC) = 0.1 dS m^{-1}, and organic carbon = 1.1%. The concentrations of the PTEs in the control with no biochar treatment (CK) were 1767.1, 14.5, 3121.2 and 1828.3 mg kg^{-1} for As, Cd, Pb, and Zn, respectively. The concentrations exceeded their maximum allowable concentrations in the soil by 88.4-time for As, 2.9-time for Cd, 10.4-time for Pb, and 6.1-time for Zn, as indicated by Kabata-Pendias (2011). The mineral components in the soil sample were studied using X-ray diffraction (XRD; X'Pert PRO MPD, PANalytical, Netherlands).

Biochars produced from three types of feedstocks, amur silvergrass (*Miscanthus sacchariflorus*), rice straw (*Oryza sativa*), and umbrella tree wood (*Maesopsis eminii*), named GBC, RBC, and WBC, respectively, were used in this study. The biochars were produced by slow pyrolysis at 500–600 °C, at a rate of 10 °C min^{-1}, and with a residence time of 1 h. The biochars were finely ground and passed through a 2-mm stainless steel sieve prior to characterization and application. More details on the biochar production method and biochar properties are described (El-Naggar et al., 2020). Furthermore, the mineral components of the biochar matrices were investigated using XRD. The surface functionalities of the biochar samples were elucidated using X-ray photoelectron spectroscopy (XPS, K-Alpha, ThermoFisher, USA). The biochar surface morphology was investigated using scanning electron microscopy (SEM; Hitachi S-4800, Japan) coupled with energy dispersive X-ray spectroscopy (EDX). The results of the soil and biochar characterizations are presented in Table S1, and detailed in the Supplementary Information.

2.2. Incubation experiment

Each biochar was applied to 100 g of soil at the rate of 22.2 g kg^{-1}, equivalent to 30 t ha^{-1} (assuming a 10-cm incorporation depth and 1.35 g cm^{-3} of soil bulk density), along with the control CK, in a high-density polyethylene bottle. The experimental units were replicated thrice. Different treatments were mixed to ensure homogeneity, and the samples were incubated at 25 °C for 473 d in an incubator (MIR-554; SANYO Electronics, Co., Ltd., Tokyo, Japan). The soil moisture level was adjusted to 70% of the soil water-holding capacity by the periodic addition of deionized water during the experiment. At the end of the incubation period, the soil samples were collected, and a portion was immediately stored at −20 °C for glomalin analysis. The remaining soil samples were air-dried, ground, and sieved to <2 mm.

2.3. Geochemical fractionation of the studied elements

The geochemical fractions of As, Cd, Pb, and Zn in addition to Fe, Mn, Al, and S were analyzed in all samples, according to the 8-step sequential extraction procedure described by El-Naggar et al. (2018b) The extracted fractions and the extraction solutions and conditions are presented in Table S2. Approximately 2 g of each air-dried soil sample was mixed with 50 mL of extractant, shaken at 20 rpm, centrifuged at 1957*g* for 10 min, and filtered through 0.45 μm membrane filters. The soil samples were digested using a microwave digestion system (Milestone; ETHOS EASY, Germany) according to standard EPA methods (US EPA, 2007), for pseudo-total element concentrations. The filtrates were preserved by adding 0.10 mL of 65% HNO_3 until analysis using inductively coupled plasma with optical emission spectrometry (ICP-OES; Ultima 2, Horiba

Jobin Yvon, Unterhaching, Germany).

2.4. Phytoavailability, potential mobility tests, and total glomalin content

The phytoavailability and potential mobility of As, Cd, Pb, and Zn were tested according to the rhizosphere-based extraction method proposed by Feng et al. (2005) and a synthetic precipitation leaching method (Hageman et al., 2000), respectively. The same procedures have been used in recent studies of contaminated soils (Beiyuan et al., 2017; El-Naggar et al., 2019b). For the phytoavailability test, a 10-mM extraction solution containing acetic, lactic, citric, malic, and formic acids (molar ratio: 4:2:1:1:1, respectively) was prepared. A 2-mL extraction solution was added to 20 mL of each soil sample, shaken for 16 h using an end-over-end shaker, and centrifuged at 1254*g* for 10 min. The samples were then filtered using disposable syringes with a 0.45-μm membrane filter and preserved by adding drops of concentrated HNO_3 until analysis. For the potential mobility test, the extraction solution was a diluted mixture of nitric and sulfuric acids (60/40 wt%) with a pH of 4.20 ± 0.05. The extraction solution was added to the soil samples at a soil-to-solution ratio of 1:20 (w:v), shaken for 18 h using an end-over-end shaker, and centrifuged at 1254*g* for 10 min. After the extractions, the samples were filtered using 0.45-μm membrane filters. The phytoavailable and potential mobile concentrations were then analyzed using the ICP-OES described above.

Total glomalin was quantified in fresh soil samples following the sodium pyrophosphate extraction method (Wright et al., 2006), using a spectrophotometer (UV-1800, Shimadzu Co., Kyoto, Japan).

2.5. X-ray absorption fine structure spectroscopy

X-ray absorption fine structure (XAFS) measurements were carried out for As at the TLS 07A1 beamline in the National Synchrotron Radiation Research Center (NSRRC) in Taiwan, and Pb at the 7D beamline in the Pohang Accelerator Laboratory (PAL) in South Korea. XAFS analysis was used to investigate the speciation of As and Pb in the control and the biochar-treated soils to elucidate the mechanisms involved in As and Pb release in different treatments. The samples were sieved through <200 mesh (0.074 mm) and distributed evenly on a Kapton tape (~4 × 2 cm) as a thin layer. Similarly, all reference compounds of As and Pb were placed on the Kapton tape for XAFS analysis. The obtained XANES data were analyzed, and the best linear combination fitting was obtained using the Athena 0.9.25 package (Ravel and Newville, 2005). The computed proportions of As and Pb speciation of the best linear combination fitting results are presented in Table S3.

2.6. X-ray photoelectron spectroscopy

At the end of the incubation period, the surface functional groups and chemical composition of soil samples were elucidated using X-ray photoelectron spectroscopy (XPS, K-Alpha, ThermoFisher, USA). In addition, Fe functional groups in the bulk soils were also investigated. As XPS is a surface-sensitive technique, strict sample preparation was followed to avoid surface contamination. To assure the quality of analysis, the binding energies of different elements were calibrated. OriginPro 9.1 software (OriginLab Corporation, Northampton, USA) was used for the smoothing of raw data of XPS results. The baseline background was subtracted to estimate the relative proportions of the chemical state likely to be present. Thereafter, the peak fitting procedure was performed using XPSPEAK41 software for spectral interpretation based on the Gaussian–Lorentzian sum function.

2.7. Quality control and data analysis

Analytical grade reagents were purchased from Sigma Aldrich for use in the analysis. Triplicate measurements were employed and values with RSD greater than 5% were excluded. The means of variables were subjected to one-way analysis of variance (ANOVA), followed by Duncan's multiple-range test at significance level of 0.05. The results of some soil parameters (pH, EC, available and water extractable PO_4^{3-}, Cl^-, SO_4^{2-}, dissolved organic carbon (DOC), dissolved aromatic carbon (DAC), cation exchange capacity (CEC), and organic carbon) at the end of this incubation experiment were reported in a previous study (El-Naggar et al., 2020). In the current study, we employed Pearson's correlation coefficient (*r*) to explore the underlying effects of the soil parameters as well as soil glomalin and the total Al, S, Fe, and Mn on the potential mobility, phytoavailability, and mobilization of the studied PTEs at significance levels of 0.01 and 0.05. All statistical analyses were conducted using IBM SPSS Statistics 24 (NY, USA).

3. Results and discussion

3.1. Geochemical fractions of As, Cd, Pb, and Zn

The mobile fractions (ΣF1-F2) accounted for 45.1% in Cd, while they were 8%, 6.8%, and 0.01% for Pb, Zn, and As, respectively, of their summation contents in the CK. The non-residual fractions (ΣF1-F7, considered as potential mobile fractions (PMF); El-Naggar et al., 2018b), were dominated by Cd and Pb, accounting for 80.9% and 61.9%, respectively, of their summation contents in the CK. Meanwhile, it accounted for only 36.3% and 43.0%, respectively, of the summation contents of As and Zn (Fig. 1). The high summation content as well as the relatively high PMF of the four PTEs pose a risk of environmental pollution in the study area.

Among the PMF of As, the amorphous and crystalline Fe oxides (F6 + F7) were the most predominant in the CK and the soils treated with different biochars. This can be attributed to the high affinity between As and Fe oxides. Pb showed the highest association with the organic matter fraction (F4) in the CK and the soils treated with different biochars among the other studied PTEs. This is ascribed to the greater adsorption of Pb by soil organic matter and its high potential to form inner-sphere metal surface complexes (Kabata-Pendias, 2011). In the case of Cd, the soluble and exchangeable fraction (F1) and the easily mobilizable fraction (F2) were the most abundant in the soils with or without biochars. The elevated mobility and easy uptake of Cd by plant roots create a potential health threat arising from the advent of toxic

elements into the food chain. It might also indicate that the Cd content could be mainly ascribed to anthropogenic origins, rather than pedogenic origins in the studied soil.

The application of biochar to the soil led to disparate changes in the geochemical fractions of PTEs. The application of RBC to the soil increased the PMF of As, Cd, Pb, and Zn by 10.3%, 3.5%, 2.5%, and 2.1%, respectively, compared to the CK. The application of GBC significantly decreased the PMF of As, Cd, Pb, and Zn by 6.0%, 3.6%, 0.5%, and 2.8%, respectively; it also led to a decrease in the soluble and exchangeable fraction (F1) of Cd and Pb by 5.4% and 9.6%, respectively, compared to the CK. While the application of WBC increased the PMF of As by 16.2%, it decreased the PMF of Cd and Pb by 5.4% and 4.0%, respectively, compared to the CK. The governing factors for the changes in the PTE geochemical fractions in the treated and untreated soils influence several aspects, which will be further discussed in Sections 3.3 and 3.4.

3.2. Phytoavailability and potential mobility of As, Cd, Pb, and Zn

The phytoavailability and potential mobility of the four PTEs showed that Zn had the highest phytoavailability, followed by As, Pb, and Cd. Meanwhile, Pb had the highest potential mobility, followed by Zn, As, and Cd. The potentially mobile concentrations of As, Cd, and Zn were lower than their phytoavailable concentrations (Fig. 2). This could be attributed to the differences in pH, as the extraction solution used in the phytoavailability test had a lower pH (1.20) than that used in the potential mobility test (pH = 4.20) and thus a stronger chelating ability for

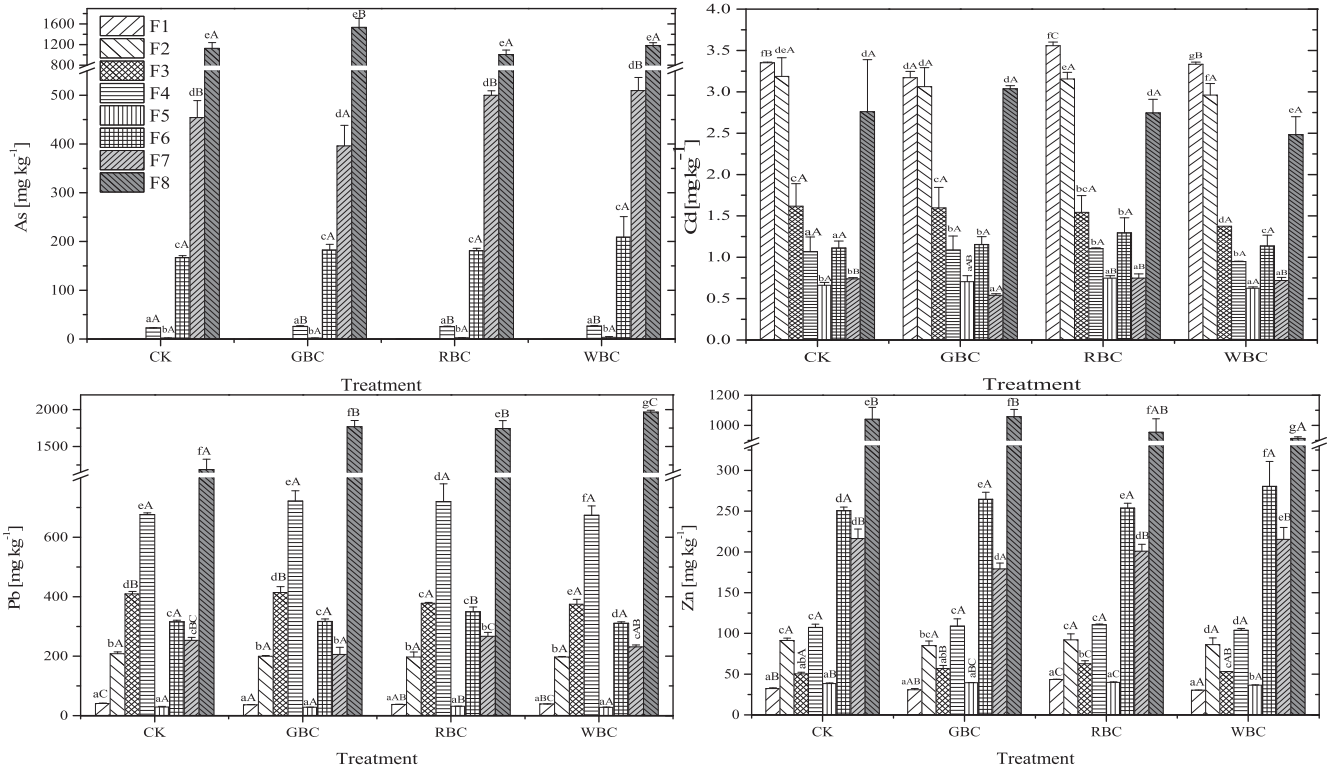

Fig. 1. Geochemical fractions of As, Cd, Pb, Zn in soils with or without different biochars. CK: control, GBC: grass biochar, RBC: rice straw biochar, WBC: wood biochar. F1: soluble + exchangeable, F2: carbonate, F3: manganese oxide, F4: organic matter (OM), F5: sulfide, F6: amorphous iron oxide, F7: crystalline iron oxide, and F8: residue. Error bars indicate the standard deviation of the mean. Different lowercase letters indicate significant ($p < 0.05$) differences in fractions among the same treatment, while uppercase letters indicate significant ($p < 0.05$) differences in the same fraction among different treatments.

the PTEs. In contrast, the phytoavailability of Pb was lower than its potential mobility. In general, Pb is known to be the least mobile element among the PTEs in the soil, and its solubility is strongly influenced by the formation of complexes with organic matter, apart from being highly dependent on the extraction solution (Kabata-Pendias, 2011). In our study, soil organic matter was the major sink of Pb; therefore, it had a major influence on its bioavailability. Consequently, the formation of Pb–organic complexes and the presence of hydroxy species of Pb (e.g., $PbOH^+$ and $Pb_4(OH_4)_4^+$) was higher when extracted with the potential mobility solution (with a higher pH), compared to that with the phytoavailability extraction solution.

The phytoavailability and potential mobility of the different elements indicated that the application of biochar to the contaminated soil did not aid in contamination remediation (Fig. 2). Among the different biochar treatments, only the WBC significantly reduced ($P < 0.05$) the phytoavailability of Zn by 16.6% compared to the CK, but this biochar had minimal effects on decreasing the phytoavailability of Cd, and Pb. This could be attributed to the high surface area (315.7 m^2 g^{-1}, Table S1), and aromatic nature of the WBC. The aromatic carbon (C═C) was the dominant C form in the WBC (62.6%), compared to other C-bonding states (Fig. 3). After biochar application to soil, O-containing functional groups (e.g., carboxyl and hydroxyl) were enriched in soils treated with WBC than that for RBC and GBC (Fig. S2), which could form surface complexes with divalent elements. On the other hand, the RBC enhanced ($P < 0.05$) the phytoavailability and potential mobility of As (by 50.4% and 61.7%, respectively), and the potential mobility of Pb and Zn (by 66.8 and 35.0%, respectively), compared to the CK. The RBC contained higher aliphatic C content as demonstrated by its high ash content (52.37%, Table S1), low fixed C (39.1%, Table S1), and high C—C/C—H (aliphatic/aromatic C) functional groups (34.6%, Fig. 3). The higher ash and aliphatic components in the RBC compared to other biochars, stimulated the release of elements associated with DOC in soil (discussed in Section 3.4).

It is worth noting that the assumed phytoavailable and potential mobile concentrations accounted for only 0.15% and 0.1% for As, 7.3% and 2.7% for Cd, 0.1% and 0.1% for Pb, and 3.7% and 0.2% for Zn, respectively. The small phytoavailable and potential mobile portions compared to the elevated total concentrations of the PTEs may reflect low ecological risk (Wang et al., 2020). However, the elements' high PMF (ΣF1-F7), obtained from sequential extraction results, demonstrated that there is high potential for considerable portions of total PTEs to be mobilized, as a response to changes in any of biogeochemical factors.

3.3. Speciation of As and Pb in biochar-treated soils

3.3.1. As

The XPS full spectrum revealed the presence of As (As3d) in the soils treated with different types of biochar (Fig. 4). The As3d spectra were deconvoluted into multi-Gaussian fitting peak components (Fig. 5a-d): As(III) when binding energy ranged between 43.7 and 44.5 eV (Navarathna et al., 2019; Wang et al., 2019) and 44.9 eV (Bang et al., 2005; Yang et al., 2017), whereas it is defined as As(V) when it ranged between 47.7 and 47.9 eV or 49.7–49.9 eV (Czanderna et al., 2002; Panda et al., 2020). As(V) was the predominant species (76.4%) at binding energies of 49.7 and 47.8 eV, while As(III) accounted for only 23.6% of its content in the CK at a binding energy of 44.5 eV. Considerable portions of the As(V) species were reduced to As(III) in the soil treated with biochars. For instance, the reduction ratio of As(V) to As(III) was 14.8% and 4.7% in the soil treated with RBC and WBC, respectively. Such transformations of As(V) to As(III) in the soils treated by biochar increase the mobility of As in the soil, as As(III) is more toxic and less stable than As (V) (Xiu et al., 2016).

The comparison of the XANES spectra of the As standards (scorodite,

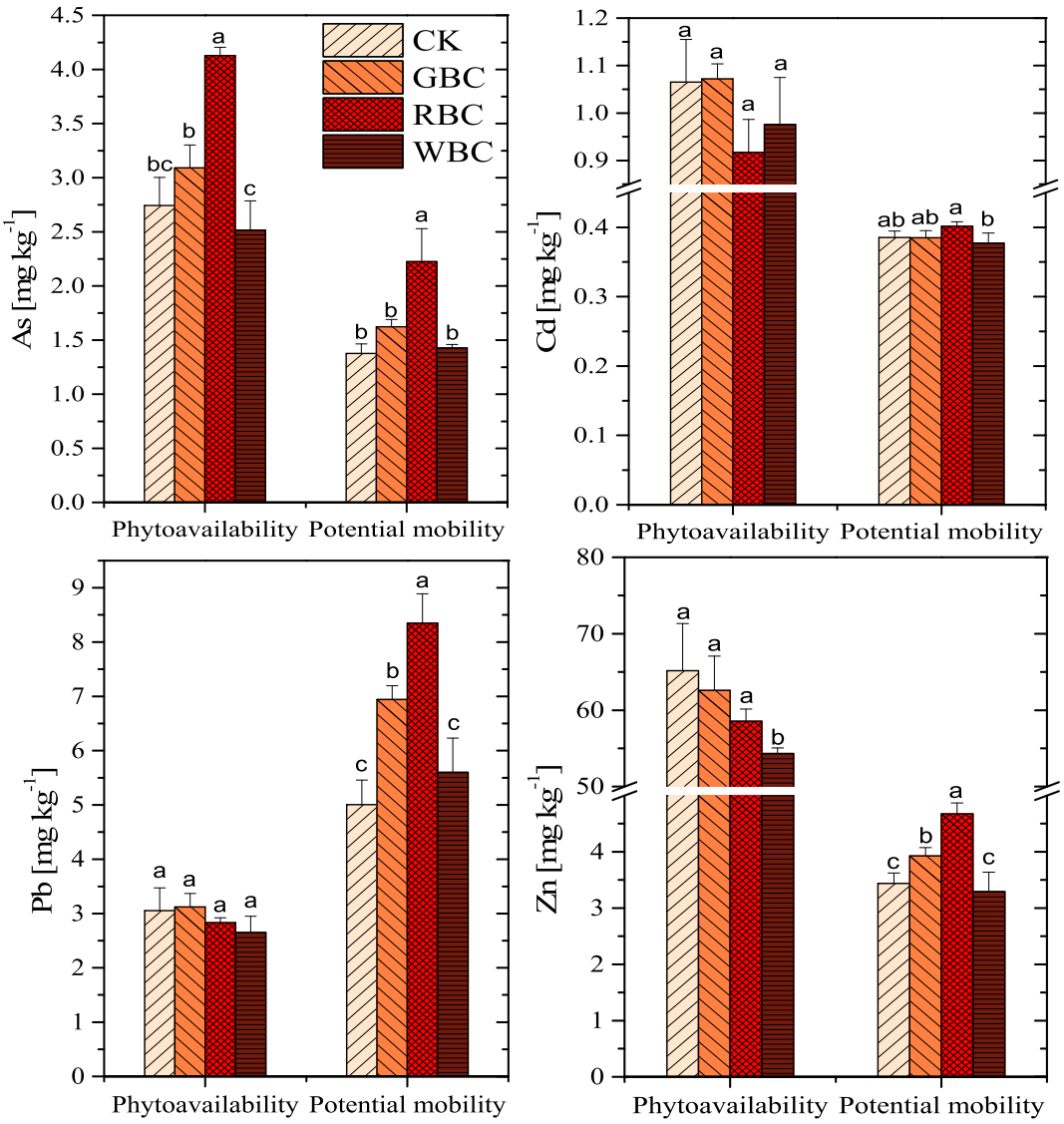

Fig. 2. Phytoavailability and potential mobility of As, Cd, Pb, Zn in soils treated with different types of biochar. Error bars indicate the standard deviation of the mean. Different letters indicate significant differences at $P < 0.05$. Please note the different scales.

arsenopyrite, goethite-As(V), goethite-As(III), ferrihydrite-As(V), and ferrihydrite-As(III)) with those of the samples was carried out using target transformation in the Athena software. It was observed that the spectra of scorodite, goethite-As(V), and ferrihydrite-As(III) were well-matched with those of the soil samples; therefore, they were selected for linear combination fitting (Fig. 6, Table S3). The linear combination fitting of the As-XANES spectra demonstrated that As in the CK was mainly dominated by scorodite; As(V) was adsorbed to goethite, while ferrihydrite-bound As was not detected (Table S3). The presence of goethite and scorodite in the CK was confirmed by the results of the XRD analysis (Fig. 4a) and the XPS spectra of Fe 2p (Fig. 4d). In the biochar-treated soils, As(III) adsorbed to goethite increased by 3–4 folds compared to the CK; in addition, significant amounts of As(III) adsorbed onto ferrihydrite were found in the soils treated with biochars (RBC: 35%, WBC: 26%, GBC: 17%).

The XANES results revealed that mineralogical transformations of Fe (hydr)oxides occurred in the biochar-treated soils, which governed the mobilization of As. In particular, the presence of biochar in the soil led to the dissolution of scorodite and the formation of less stable forms of Fe (hydr)oxides-bound As (with goethite and ferrihydrite). The presence of goethite in the soil significantly reduces the stability of scorodite and promotes its dissolution to less stable forms (Harvey et al., 2006). When the soil samples were treated with the biochars, they potentially promoted the reduction of As(V) to As(III) due to the presence of electron-donor functional groups on the surfaces of the biochar and/or in the biochar-derived DOC, such as eCOOH and phenolic OH (Niazi et al., 2018). Hence, the results of XPS and XANES consistently confirmed the reduction of As(V) to As(III) in the biochar-treated soils. This was especially true in the soil treated with RBC, which increased the potential mobility and phytoavailability of As (Fig. 2).

3.3.2. Pb

The high-resolution Pb 4f XPS spectra was deconvoluted into peak components (Fig. 5e-h) (Tan et al., 2019; Yang et al., 2018; Zhang et al., 2019). The fitted curve for the XPS spectra of samples from the CK treatment revealed several Pb(II) functional groups, such as $PbCO_3$/$Pb(OH)_2$ (137.7–138.2 eV, 37.3%), Pb^{2+} (139.3–139.9 eV, 16.4%), and PbO (142.8–143.1 eV, 46.3%). In soils treated with biochar, Pb^{2+} was converted to O-containing functional groups (PbO, $PbCO_3$/$Pb(OH)_2$); Pb^{2+} accounted for 16.4% in CK, but only accounted for 4.1%, 4.8%, and 0% in the soils treated with GBC, RBC, and WBC, respectively. This reduction in Pb^{2+} was in line with the increase of other Pb species (PbO, $PbCO_3$/$Pb(OH)_2$). The XPS data of C1s for the three types of biochar samples showed the presence of C═O and C—O/O—H on the biochar

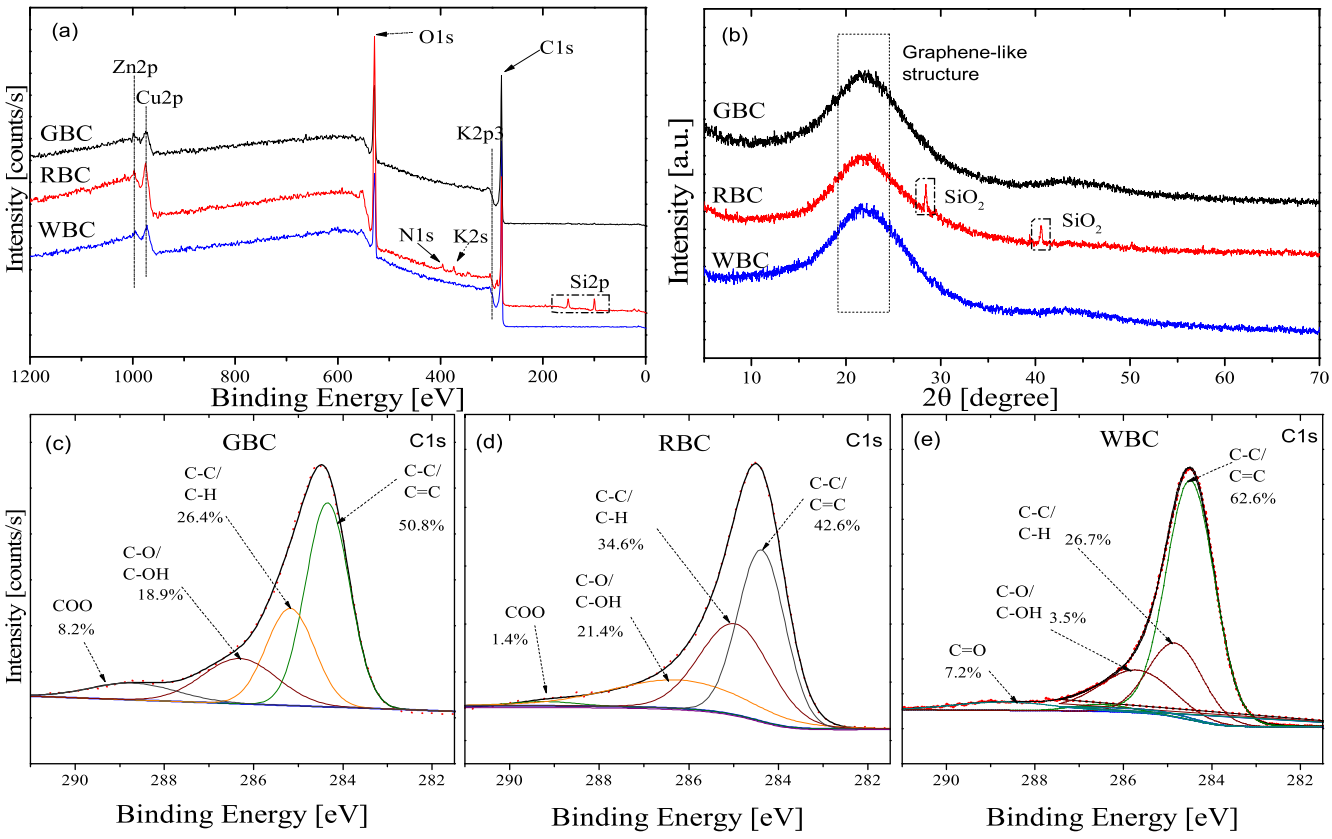

Fig. 3. Biochar characterization using a) XRD, b) XPS survey scan, and c-e) the deconvoluted C1s peaks of grass biochar (GBC), rice straw biochar (RBC), and wood biochar (WBC). Red dotted line: experimental data; thick black line: sum of fitted curve; blue line: background. Others are Gaussian fitting curves. (For interpretation of the references to colour in this figure legend, the reader is referred to the web version of this article.)

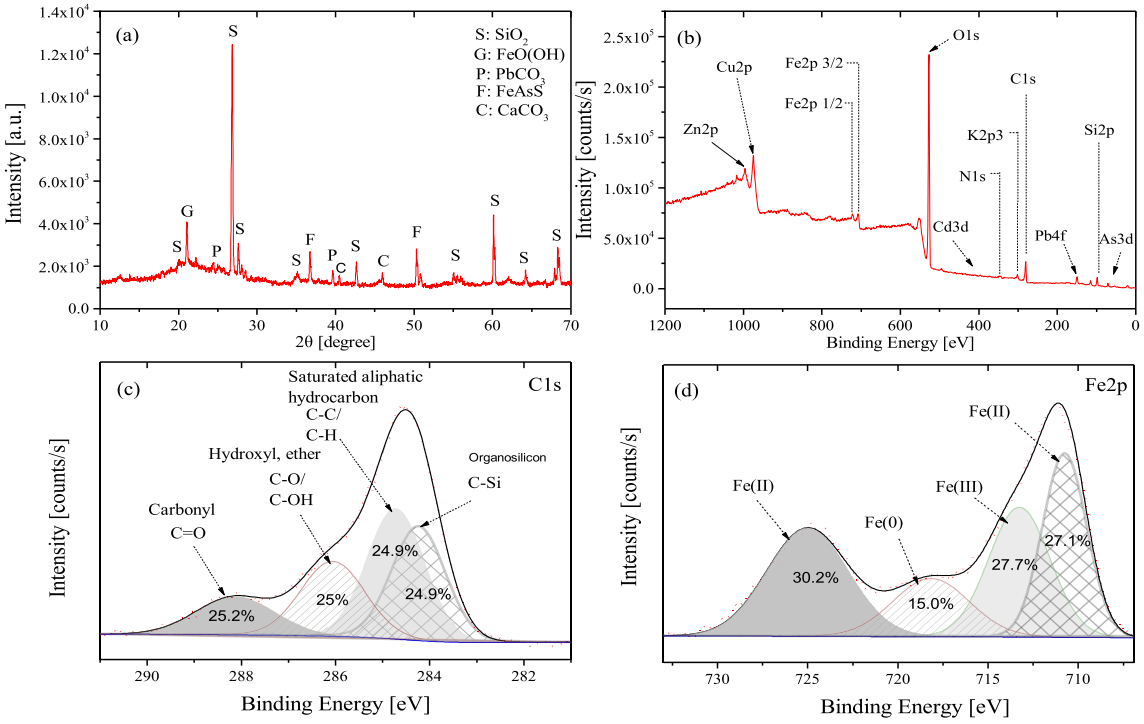

Fig. 4. Soil characterization using a) XRD, b) XPS survey scan, and c) the deconvoluted C1s peak, d) the deconvoluted Fe 2p peak. Red dotted line: experimental data; black thick line: sum of fitted curve; blue line: background. Others are Gaussian fitting curves. (For interpretation of the references to colour in this figure legend, the reader is referred to the web version of this article.)

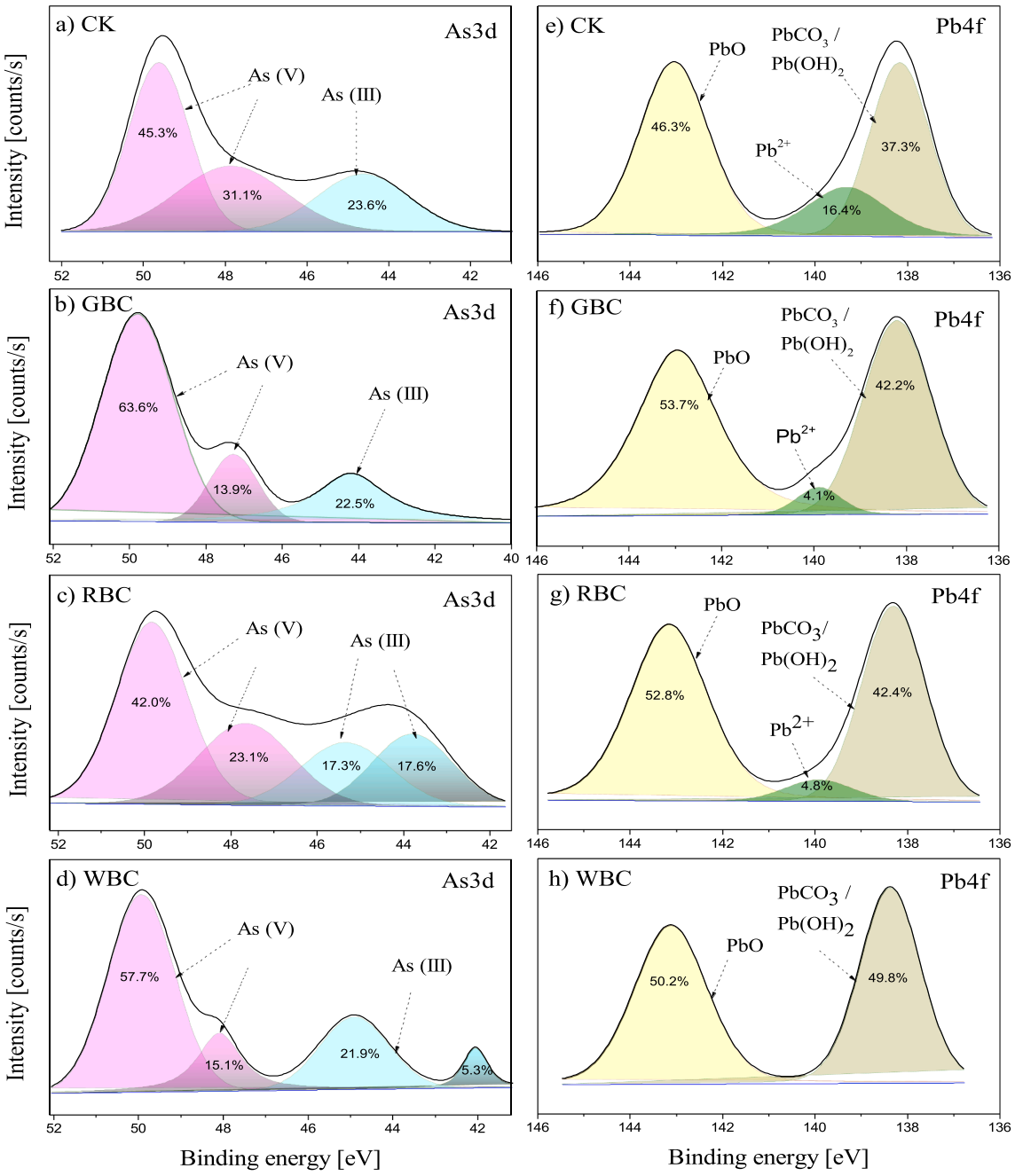

Fig. 5. XPS deconvoluted As 3d peak (a–d) and Pb 4f peak (e–h) of the soils treated with different biochars. Red dotted line: experimental data; black thick line: sum of fitted curve; blue line: background. Others are Gaussian fitting curves. (For interpretation of the references to colour in this figure legend, the reader is referred to the web version of this article.)

surface, especially the GBC, which contained the highest ratio (34.2%) of both forms (Fig. 4c-e). Therefore, we concluded that the phenolic hydroxyl and carboxylic groups of biochar surfaces promoted the conversion of Pb from Pb^{2+} into $PbCO_3$/$Pb(OH)_2$ and/or PbO. The role of the phenolic hydroxyl and carboxylic groups in the transformation of Pb (II) in the soil has been previously reported (Zhang et al., 2017). Pb species in soils with and without biochar was further determined using Pb L_3-edge XANES spectroscopy (Fig. 6b). The linear combination fitting results of Pb-XANES spectra demonstrated that Pb in the CK was mainly adsorbed on humic acid (88.5%, Table S3). Pb had a high binding affinity with organic matter in the studied soil, as recorded from the sequential extraction (Fig. 1). In addition, the dissolved organic matter in the studied soil originated from humic-like substances (El-Naggar et al., 2020). Apart from humic acid, Pb was also bound to cerussite (11.5%) in the CK, as indicated by the linear combination fitting results. Additionally, the presence of cerussite in the studied soil was supported by the X-ray diffractogram (Fig. 4b). In general, cerussite is stable and has low solubility ($K_{sp}(PbCO_3) = 7.45 \times 10^{-14}$) (Beiyuan et al., 2020). However, $PbCO_3$ decreased significantly in the soil treated with GBC, accounting for a meager 6.2%, while the content of hydrocerussite was 14.6%. This could be attributed to the presence of large amounts of carbonyl and hydroxyl groups on the surfaces of GBC, which enhanced the CO_3^{2-} hydrolysis. In the soil treated with RBC, the Pb bound to cerussite was reduced to 7%, while the Pb adsorbed on humic acid increased to 93%. This might be because the soil treated with RBC had the highest terrestrial humic-like substances compared to GBC and WBC, as reported by El-Naggar et al. (2020). In contrast, the soil treated with WBC exhibited the highest cerussite ratio (19.2%), compared to the soils

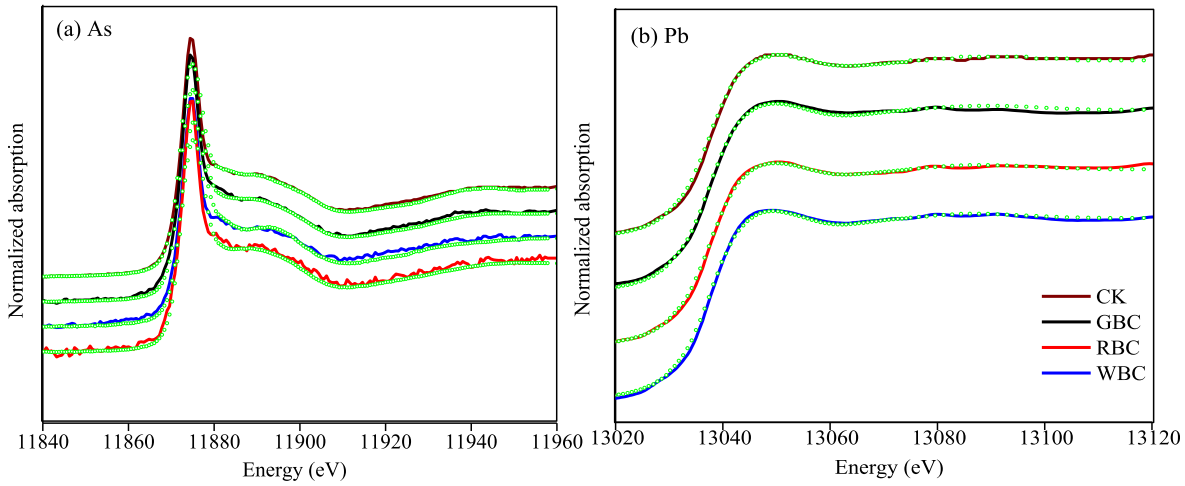

Fig. 6. Linear combination fitting of (a) As-XANES and (b) Pb-XANES results of soils treated with different biochars. Normalized spectra: solid lines; fitting: dotted lines.

treated with GBC and RBC, thus demonstrating a greater stability of Pb with the WBC treatment. This result agrees with the Pb4f XPS spectra (Fig. 5h), which exhibited higher proportions of $PbCO_3$/$Pb(OH)_2$ and PbO in the soil treated with WBC compared to the CK, resulting in lower phytoavailability and potential mobility compared to the other biochar treatments (Fig. 1).

3.4. Factors controlling As, Cd, Pb, and Zn behavior in biochar-treated soils

The phytoavailability and potential mobility of As were positively correlated with DOC ($r = 0.903$ and 0.846, respectively, $P < 0.01$) and DAC ($r = 0.880$ and 0.878, respectively, $P < 0.01$) (Fig. 7; Table S4). Moreover, the ratio of the mobile fraction to the summation (MF/SUM) of As was positively correlated with DOC ($r = 0.739$, $P < 0.01$) and DAC ($r = 0.818$, $P < 0.01$); additionally, the ratio of PMF to the summation (PMF/SUM) of As was positively correlated with DOC ($r = 0.597$, $P < 0.05$). These relationships demonstrate the vital role of biochar-derived DOC and DAC in enhancing the mobilization and phytoavailability of As, especially in the soils treated with RBC and GBC. As has affinity with organic matter components to form complexes via Fe bridging; therefore, we hypothesized that the release of DOC and DAC prompted the conversion of As into more available forms and their subsequent release. This explains the role of biochar in enhancing As mobilization, particularly in the RBC treated soil, which contained the highest contents of ash and aliphatic functional groups. Furthermore, the As phytoavailability, potential mobility, and MF/SUM exhibited positive relationships with Cl^- and SO_4^{2-} (r ranged between 0.662 and 0.909, $P < 0.05$). This suggests that the increased concentrations of Cl^- and SO_4^{2-} in biochar-treated soils led to higher mobility of As in the soil solution, as previously reported (Ahmad et al., 2017). The available phosphorus (A-PO_4^{3-}) and water extractable phosphorus (WE-PO_4^{3-}) were positively correlated

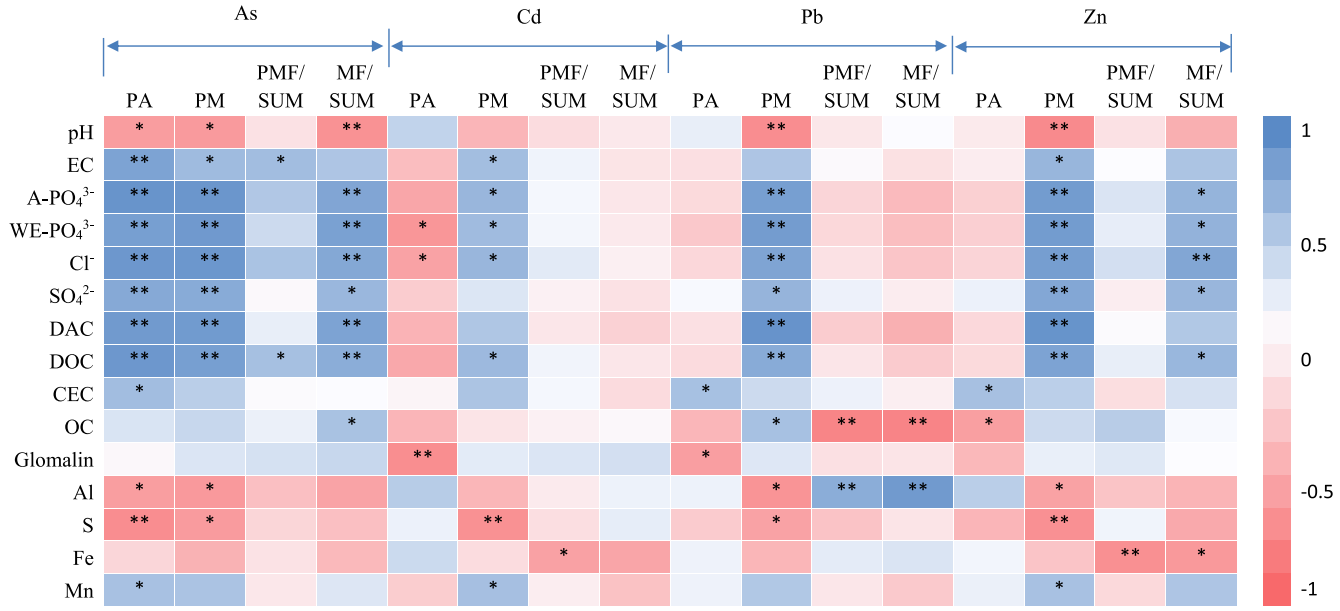

Fig. 7. Heatmap of the association between phytoavailability (PA), potential mobility (PM), ratio of potential mobile fractions (ΣF1-F7) to summation of the eight geochemical fractions (PMF/SUM), ratio of mobile fractions (F1 + F2) to SUM (MF/SUM) of the elements and the relevant controlling factors. The pH, EC, available phosphorus (A-PO_4^{3-}), water extractable phosphorus (WE-PO_4^{3-}), Cl^-, SO_4^{2-}, dissolved organic carbon (DOC), dissolved aromatic carbon (DAC), cation exchange capacity (CEC), and organic carbon (OC) data are from a previous study (El-Naggar et al., 2020).* Correlation is significant at the 0.05 level. ** Correlation is significant at the 0.01 level.

with the As phytoavailability, potential mobility, and MF/SUM (r ranged from 0.797 to 0.927, $P < 0.01$). Competition between As and PO_4^{3-} for sorption sites has already been reported in soils treated with biochar (Igalavithana et al., 2017). The RBC had the highest P content compared to GBC and WBC (Table S1), thus enhancing the mobilization and phytoavailability of As. In addition, the pH was negatively correlated with the As phytoavailability, potential mobility, and MF/SUM (r ranged from −0.630 to −0.716, $P < 0.05$). It has been reported that the negatively charged acidic functional groups on biochar surfaces may facilitate the dissolution of As and stimulate the release of As into the soil (El-Naggar et al., 2019b).

Cationic PTEs (Cd, Pb, and Zn) exhibited analogical interactions with the potential controlling factors. The potential mobilities of Cd, Pb, and Zn were positively correlated with DOC, and the potential mobilities of Cd and Pb were positively correlated with DAC. These relationships confirm the role of dissolved organic compounds in the release of Pb into the soil solution, based on the sequential extraction and XANES results. Recent studies reported the influence of DOC and DAC on the (im) mobilization of Pb (Beiyuan et al., 2020) as well as Cd and Zn (El-Naggar et al., 2018b). The release of dissolved aromatic and aliphatic compounds into the soil facilitates the mobilization of associated cationic PTEs. Furthermore, the potential mobility (PM) of Cd and Zn exhibited a positive correlation with Mn, suggesting that the dissolution of Mn oxides may lead to the release of adsorbed and coprecipitated Cd and Zn.

Interestingly, the results of the Pearson's correlation analysis showed negative correlations between S and the PM of Cd, Pb, and Zn, while SO_4^{2-} exhibited positive correlations with Pb and Zn. This suggests that when sulfides are transformed to sulfates in the soil, the associated elements are released into the soil solution. Notably, A-PO_4^{3-} and WE-PO_4^{3-} also showed positive correlations with the PM of Cd, Pb, and Zn, suggesting that the three cations were associated with PO_4^{3-}; thus, its release into the soil solution led to the release of the toxic elements. This clarifies the elevated PM of Cd, Pb, and Zn in the soil treated with RBC compared to the other treatments, which can be attributed to the greater total P content in the RBC. The phytoavailability of Cd and Pb was negatively correlated with glomalin. Our results also showed that the biochar-induced increase in glomalin was associated with a decrease in the phytoavailability of Cd and Pb, as indicated by the negative correlations. Glomalin, which is produced by the hyphae of arbuscular mycorrhizal fungi, is known to sequester PTEs, reducing their uptake by plant roots (González-Chávez et al., 2004). This could explain the enhanced performance of biochar in reducing the phytoavailability of the elements instead of their mobility (Fig. 2). Remarkably, the phytoavailability of Pb and Zn exhibited positive correlations with the CEC; this was contradictory to the expected behavior. One of the key properties of biochar, which increases its potential to immobilize the cationic elements, is promoting the CEC in soil, which in turn affords an enhanced capacity for PTE adsorption (El-Naggar et al., 2018a; Zama et al., 2018). This anomalous behavior (positive correlation with CEC) could be explained by the competitive sorption of the different cationic contaminants on the exchange sites of the biochar surfaces; this led to the lower retaining potential in multi-contaminated soils.

4. Conclusions

The studied soil was highly multi-contaminated, with high potential mobile fractions of Cd and Pb, and low potential mobile fractions of As and Zn. The potential of the three studied biochars, having a wide range of differences in their properties, to remediate the multi-contaminated soil was low. Different biochars produced from different feedstocks behave distinctively for the (im)mobilization of toxic elements in multi-contaminated soils. A number of factors control the (im)mobilization of toxic elements in soils. These factors include the release of DOC, DAC, Cl^-, Fe, and Mn, S-SO_4^{2-} chemistry, phosphate competition, electrostatic repulsion, and kinetics of mineral dissolution and the release of associated elements into less stable forms. Moreover, different multi-cationic toxic elements compete for the exchange sites of biochar surfaces; this leads to a decreased potential for retaining the elements in multi-contaminated soils. Additionally, the negatively charged acidic functional groups on biochar surfaces play a crucial role in the dissolution of coprecipitated toxic elements as they act as electron donors and, for instance, promote the transformation of As (V) to As (III), and Pb^{2+} to $PbCO_3$/$Pb(OH)_2$ and/or PbO. Therefore, the application of biochar to soils with a high mobilization potential of multi-contaminants remains a challenge for the biochar field applications. Based on our results that show that none of the applied biochar had positive effects on detracting the mobilization of the elements, the application of such pristine biochar to remediate such soils with elevated concentrations of multi-contaminants is not recommended. Therefore, the optimization of biochar properties by designing higher surface area and functionality, and provision of active sites for capturing PTEs is essential before it is suitable for application in multi-contaminated soil remediation.

Author contribution

Ali El-Naggar: Conceptualization, Data curation, Formal analysis, Methodology, Results interpretation, Writing - original draft. **Scott X. Chang:** Results interpretation, Methodology, Validation, Visualization, Writing - review & editing. **Yanjiang Cai:** Results interpretation, Methodology, Validation, Visualization, Writing - review & editing. **Young Han Lee:** Results interpretation, Methodology, Validation, Visualization, Writing - review & editing. **Jianxu Wang:** Results interpretation, Methodology, Validation, Visualization, Writing - review & editing. **Shan-Li Wang:** Results interpretation, Methodology, Validation, Visualization, Writing - review & editing. **Changkook Ryu:** Results interpretation, Methodology, Validation, Visualization, Writing - review & editing. **Jörg Rinklebe:** Conceptualization, Funding acquisition, Supervision, Validation, Results interpretation, Writing - review & editing. **Yong Sik Ok:** Conceptualization, Funding acquisition, Supervision, Validation, Results interpretation, Writing - review & editing.

Declaration of Competing Interest

The authors declare that they have no known competing financial interests or personal relationships that could have appeared to influence the work reported in this paper.

Acknowledgments

This work was carried out with the support of "Cooperative Research Program for Agriculture Science and Technology Development (Project No. PJ01475801)", Rural Development Administration, Republic of Korea. This study was also supported by the National Research Foundation of Korea (NRF) (Germany-Korea Partnership Program (GEnKO Program) 2018–2020 and NRF-2015R1A2A2A11001432) and a Korea University Grant. The XAFS spectroscopy analysis was in part conducted using a Beamline 7D at Pohang Accelerator Laboratory (PAL). The authors are also grateful to the National Synchrotron Radiation Research Center (NSRRC) and in particular Dr. Soo, Yun-Liang (TLS 07A1), and Dr. Lee, Jyh-Fu (TLS 17C1).

Appendix A. Supplementary material

Supplementary data to this article can be found online at https://doi.org/10.1016/j.envint.2021.106638.

References

Ahmad, M., Lee, S.S., Lee, S.E., Al-Wabel, M.I., Tsang, D.C.W., Ok, Y.S., 2017. Biochar-induced changes in soil properties affected immobilization/mobilization of metals/metalloids in contaminated soils. J. Soils Sediments 17, 717–730. https://doi.org/10.1007/s11368-015-1339-4.

Ahmad, M., Rajapaksha, A.U., Lim, J.E., Zhang, M., Bolan, N., Mohan, D., Vithanage, M., Lee, S.S., Ok, Y.S., 2014. Biochar as a sorbent for contaminant management in soil and water: a review. Chemosphere 99, 19–33. https://doi.org/10.1016/j.chemosphere.2013.10.071.

Awad, Y.M., Ok, Y.S., Abrigata, J., Beiyuan, J., Beckers, F., Tsang, D.C.W., Rinklebe, J., 2018. Pine sawdust biomass and biochars at different pyrolysis temperatures change soil redox processes. Sci. Total Environ. 625, 147–154. https://doi.org/10.1016/J.SCITOTENV.2017.12.194.

Bang, S., Johnson, M.D., Korfiatis, G.P., Meng, X., 2005. Chemical reactions between arsenic and zero-valent iron in water. Water Res. 39, 763–770. https://doi.org/10.1016/j.watres.2004.12.022.

Beiyuan, J., Awad, Y.M., Beckers, F., Tsang, D.C.W., Ok, Y.S., Rinklebe, J., 2017. Mobility and phytoavailability of As and Pb in a contaminated soil using pine sawdust biochar under systematic change of redox conditions. Chemosphere 178, 110–118. https://doi.org/10.1016/j.chemosphere.2017.03.022.

Beiyuan, J., Awad, Y.M., Beckers, F., Wang, J., Tsang, D.C.W., Ok, Y.S., Wang, S.L., Wang, H., Rinklebe, J., 2020. (Im)mobilization and speciation of lead under dynamic redox conditions in a contaminated soil amended with pine sawdust biochar. Environ. Int. 135, 105376. https://doi.org/10.1016/j.envint.2019.105376.

Czanderna, A., Madey, T., Powell, C., 2002. Beam effects, surface topography, and depth profiling in surface analysis, beam effects, surface topography, and depth profiling in surface. Analysis. https://doi.org/10.1007/b119182.

El-Naggar, A., Lee, M.H., Hur, J., Lee, Y.H., Igalavithana, A.D., Shaheen, S.M., Ryu, C., Rinklebe, J., Tsang, D.C.W., Ok, Y.S., 2020. Biochar-induced metal immobilization and soil biogeochemical process: an integrated mechanistic approach. Sci. Total Environ. 698, 134112. https://doi.org/10.1016/j.scitotenv.2019.134112.

El-Naggar, A., Lee, S.S., Rinklebe, J., Farooq, M., Song, H., Sarmah, A.K., Zimmerman, A. R., Ahmad, M., Shaheen, S.M., Ok, Y.S., 2019a. Biochar application to low fertility soils: a review of current status, and future prospects. Geoderma 337, 536–554. https://doi.org/10.1016/j.geoderma.2018.09.034.

El-Naggar, A., Rajapaksha, A.U., Shaheen, S.M., Rinklebe, J., Ok, Y.S., 2018a. Potential of biochar to immobilize nickel in contaminated soils. In: Nickel in Soils and Plants. CRC Press, pp. 293–318. https://doi.org/10.1201/9781315154664-13.

El-Naggar, A., Shaheen, S.M., Hseu, Z.-Y., Wang, S.-L., Ok, Y.S., Rinklebe, J., 2019b. Release dynamics of As Co, and Mo in a biochar treated soil under pre-definite redox conditions. Sci. Total Environ. 657, 686–695. https://doi.org/10.1016/J.SCITOTENV.2018.12.026.

El-Naggar, A., Shaheen, S.M., Ok, Y.S., Rinklebe, J., 2018b. Biochar affects the dissolved and colloidal concentrations of Cd, Cu, Ni, and Zn and their phytoavailability and potential mobility in a mining soil under dynamic redox-conditions. Sci. Total Environ. 624, 1059–1071. https://doi.org/10.1016/j.scitotenv.2017.12.190.

Feng, M.H., Shan, X.Q., Zhang, S., Wen, B., 2005. A comparison of the rhizosphere-based method with DTPA, EDTA, CaCl 2, and NaNO3 extraction methods for prediction of bioavailability of metals in soil to barley. Environ. Pollut. 137, 231–240. https://doi.org/10.1016/j.envpol.2005.02.003.

González-Chávez, M.C., Carrillo-González, R., Wright, S.F., Nichols, K.A., 2004. The role of glomalin, a protein produced by arbuscular mycorrhizal fungi, in sequestering potentially toxic elements. Environ. Pollut. 130, 317–323. https://doi.org/10.1016/j.envpol.2004.01.004.

Hageman, P.L., Briggs, P.H., Desborough, G. a, Lamothe, P.J., Theodorakos, P.J., 2000. Synthetic Precipitation Leaching Procedure (splp) leachate chemistry data for solid mine- waste composite samples from Southwestern New Mexico, and Leadville, Colorado. U.S. Geol. Surv., pp. 22.

Harvey, M.C., Schreiber, M.E., Rimstidt, J.D., Griffith, M.M., 2006. Scorodite dissolution kinetics: Implications for arsenic release. Environ. Sci. Technol. 40, 6709–6714. https://doi.org/10.1021/es061399f.

Hou, D., O'Connor, D., Igalavithana, A.D., Alessi, D.S., Luo, J., Tsang, D.C.W., Sparks, D. L., Yamauchi, Y., Rinklebe, J., Ok, Y.S., 2020. Metal contamination and bioremediation of agricultural soils for food safety and sustainability. Nat. Rev. Earth Environ. 1, 366–381. https://doi.org/10.1038/s43017-020-0061-y.

Igalavithana, A.D., Kwon, E.E., Vithanage, M., Rinklebe, J., Moon, D.H., Meers, E., Tsang, D.C.W., Ok, Y.S., 2019. Soil lead immobilization by biochars in short-term laboratory incubation studies. Environ. Int. 127, 190–198. https://doi.org/10.1016/j.envint.2019.03.031.

Igalavithana, A.D., Lee, S.-E., Lee, Y.H., Tsang, D.C.W., Rinklebe, J., Kwon, E.E., Ok, Y.S., Lee, S.-E., Rinklebe, J., Kwon, E.E., Igalavithana, A.D., Tsang, D.C.W., Ok, Y.S., 2017. Heavy metal immobilization and microbial community abundance by vegetable waste and pine cone biochar of agricultural soils. Chemosphere 174, 593–603. https://doi.org/10.1016/j.chemosphere.2017.01.148.

Kabata-Pendias, A., 2011. Trace Elements in Soils and Plants. CRC Press.

Lu, H.P., Li, Z.A., Gascó, G., Méndez, A., Shen, Y., Paz-Ferreiro, J., 2018. Use of magnetic biochars for the immobilization of heavy metals in a multi-contaminated soil. Sci. Total Environ. 622–623, 892–899. https://doi.org/10.1016/j.scitotenv.2017.12.056.

Masto, R.E., Singh, M.K., Rout, T.K., Kumar, A., Kumar, S., George, J., Selvi, V.A., Dutta, P., Tripathi, R.C., Srivastava, N.K., 2019. Health risks from PAHs and potentially toxic elements in street dust of a coal mining area in India. Environ. Geochem. Health 41, 1923–1937. https://doi.org/10.1007/s10653-019-00250-5.

Monteiro, N.B.R., da Silva, E.A., Moita Neto, J.M., 2019. Sustainable development goals in mining. J. Clean. Prod. 228, 509–520. https://doi.org/10.1016/j.jclepro.2019.04.332.

Navarathna, C.M., Karunanayake, A.G., Gunatilake, S.R., Pittman, C.U., Perez, F., Mohan, D., Mlsna, T., 2019. Removal of Arsenic(III) from water using magnetite precipitated onto Douglas fir biochar. J. Environ. Manage. 250, 109429. https://doi.org/10.1016/j.jenvman.2019.109429.

Niazi, N.K., Bibi, I., Shahid, M., Ok, Y.S., Burton, E.D., Wang, H., Shaheen, S.M., Rinklebe, J., Lüttge, A., 2018. Arsenic removal by perilla leaf biochar in aqueous solutions and groundwater: an integrated spectroscopic and microscopic examination. Environ. Pollut. 232, 31–41. https://doi.org/10.1016/j.envpol.2017.09.051.

Palansooriya, K.N., Shaheen, S.M., Chen, S.S., Tsang, D.C.W., Hashimoto, Y., Hou, D., Bolan, N.S., Rinklebe, J., Ok, Y.S., 2020. Soil amendments for immobilization of potentially toxic elements in contaminated soils: a critical review. Environ. Int. 134, 105046. https://doi.org/10.1016/j.envint.2019.105046.

Panda, A.P., Rout, P., Kumar, S.A., Jha, U., Swain, S.K., 2020. Enhanced performance of a core-shell structured Fe(0)@Fe oxide and Mn(0)@Mn oxide (ZVIM) nanocomposite towards remediation of arsenic contaminated drinking water. J. Mater. Chem. A 8, 4318–4333. https://doi.org/10.1039/d0ta00611d.

Pukalchik, M., Mercl, F., Panova, M., Břendová, K., Terekhova, V.A., Tlustoš, P., 2017. The improvement of multi-contaminated sandy loam soil chemical and biological properties by the biochar, wood ash, and humic substances amendments. Environ. Pollut. 229, 516–524. https://doi.org/10.1016/j.envpol.2017.06.021.

Pukalchik, M., Mercl, F., Terekhova, V., Tlustoš, P., 2018. Biochar, wood ash and humic substances mitigating trace elements stress in contaminated sandy loam soil: evidence from an integrative approach. Chemosphere 203, 228–238. https://doi.org/10.1016/j.chemosphere.2018.03.181.

Rajapaksha, A.U., Chen, S.S., Tsang, D.C.W., Zhang, M., Vithanage, M., Mandal, S., Bolan, N.S., Sik Ok, Y., 2016. Engineered/designer biochar for contaminant removal/immobilization from soil and water: potential and implication of biochar modification. Chemosphere 148, 276–291. https://doi.org/10.1016/j.chemosphere.2016.01.043.

Ravel, B., Newville, M., 2005. ATHENA, ARTEMIS, HEPHAESTUS: data analysis for X-ray absorption spectroscopy using IFEFFIT. J. Sync. Radiat. 537–541. https://doi.org/10.1107/S0909049505012719.

Rinklebe, J., Antoniadis, V., Shaheen, S.M., Rosche, O., Altermann, M., 2019. Health risk assessment of potentially toxic elements in soils along the Central Elbe River. Germany. Environ. Int. 126, 76–88. https://doi.org/10.1016/J.ENVINT.2019.02.011.

Shaheen, S.M., El-Naggar, A., Wang, J., Hassan, N.E.E., Niazi, N.K., Wang, H., Tsang, D. C.W., Ok, Y.S., Bolan, N., Rinklebe, J., 2018. Biochar as an (Im)mobilizing Agent for the Potentially Toxic Elements in Contaminated Soils, in: Biochar from Biomass and Waste. Elsevier, pp. 255–274. https://doi.org/10.1016/b978-0-12-811729-3.00014-5.

Shaheen, S.M., Niazi, N.K., Hassan, N.E.E., Bibi, I., Wang, H., Tsang, D.C.W., Ok, Y.S., Bolan, N., Rinklebe, J., 2019. Wood-based biochar for the removal of potentially toxic elements in water and wastewater: a critical review. Int. Mater. Rev. 64, 216–247. https://doi.org/10.1080/09506608.2018.1473096.

Sun, Y., Yu, I.K.M., Tsang, D.C.W., Cao, X., Lin, D., Wang, L., Graham, N.J.D., Alessi, D.S., Komárek, M., Ok, Y.S., Feng, Y., Li, X.D., 2019. Multifunctional iron-biochar composites for the removal of potentially toxic elements, inherent cations, and hetero-chloride from hydraulic fracturing wastewater. Environ. Int. 124, 521–532. https://doi.org/10.1016/j.envint.2019.01.047.

Tan, G., Liu, Y., Xiao, D., 2019. Preparation of manganese oxides coated porous carbon and its application for lead ion removal. Carbohydr. Polym. 219, 306–315. https://doi.org/10.1016/j.carbpol.2019.04.058.

US EPA, 2007. METHOD 3051A: Microwave assisted acid digestion of sediments, sludges, soils, and oils. Test Methods Eval. Solid Waste.

Wang, J., Zeng, X., Xu, D., Gao, L., Li, Y., Gao, B., 2020. Chemical fractions, diffusion flux and risk assessment of potentially toxic elements in sediments of Baiyangdian Lake. China. Sci. Total Environ. 724, 138046. https://doi.org/10.1016/j.scitotenv.2020.138046.

Wang, L., Chen, L., Tsang, D.C.W., Zhou, Y., Rinklebe, J., Song, H., Kwon, E.E., Baek, K., Sik Ok, Y., 2019. Mechanistic insights into red mud, blast furnace slag, or metakaolin-assisted stabilization/solidification of arsenic-contaminated sediment. Environ. Int. 133, 105247. https://doi.org/10.1016/j.envint.2019.105247.

Wright, S.F., Nichols, K.A., Schmidt, W.F., 2006. Comparison of efficacy of three extractants to solubilize glomalin on hyphae and in soil. Chemosphere 64, 1219–1224. https://doi.org/10.1016/j.chemosphere.2005.11.041.

Xiu, W., Guo, H., Shen, J., Liu, S., Ding, S., Hou, W., Ma, J., Dong, H., 2016. Stimulation of Fe(II) oxidation, biogenic lepidocrocite formation, and arsenic immobilization by Pseudogulbenkiania Sp. Strain 2002. Environ. Sci. Technol. 50, 6449–6458. https://doi.org/10.1021/acs.est.6b00562.

Yang, K., Lou, Z., Fu, R., Zhou, J., Xu, J., Baig, S.A., Xu, X., 2018. Multiwalled carbon nanotubes incorporated with or without amino groups for aqueous Pb(II) removal: comparison and mechanism study. J. Mol. Liq. 260, 149–158. https://doi.org/10.1016/j.molliq.2018.03.082.

Yang, M., Jiang, T.J., Wang, Y., Liu, J.H., Li, L.N., Chen, X., Huang, X.J., 2017. Enhanced electrochemical sensing arsenic(III) with excellent anti-interference using amino-functionalized graphene oxide decorated gold microelectrode: XPS and XANES evidence. Sens. Actuators, B Chem. 245, 230–237. https://doi.org/10.1016/j.snb.2017.01.139.

You, S., Ok, Y.S., Chen, S.S., Tsang, D.C.W., Kwon, E.E., Lee, J., Wang, C.H., 2017. A critical review on sustainable biochar system through gasification: energy and environmental applications. Bioresour. Technol. https://doi.org/10.1016/j.biortech.2017.06.177.

Yuan, Y., Bolan, N., Prévoteau, A., Vithanage, M., Biswas, J.K., Wang, H., 2017. Applications of biochar in redox-mediated reactions. Bioresour. Technol. 246, 271–281. https://doi.org/10.1016/J.BIORTECH.2017.06.154.

Zama, E.F., Reid, B.J., Arp, H.P.H., Sun, G.X., Yuan, H.Y., Zhu, Y.G., 2018. Advances in research on the use of biochar in soil for remediation: a review. J. Soils Sediments 18, 2433–2450. https://doi.org/10.1007/s11368-018-2000-9.

Zhang, C., Shan, B., Tang, W., Zhu, Y., 2017. Comparison of cadmium and lead sorption by Phyllostachys pubescens biochar produced under a low-oxygen pyrolysis atmosphere. Bioresour. Technol. 238, 352–360. https://doi.org/10.1016/j.biortech.2017.04.051.

Zhang, J., Shao, J., Jin, Q., Li, Z., Zhang, X., Chen, Y., Zhang, S., Chen, H., 2019. Sludge-based biochar activation to enhance Pb(II) adsorption. Fuel 252, 101–108. https://doi.org/10.1016/j.fuel.2019.04.096.